August 19-22, 2013, Boston, MA
AIAA Atmospheric Flight Mechanics (AFM) Conference

Hybrid Exact-Approximate Analytic Hypersonic Aerodynamic Relations for General Vehicle Shapes

Michael J. Grant*
Purdue University, West Lafayette, IN, 47906

This study investigates the creation of hybrid exact-approximate, analytic hypersonic aerodynamic relations for a wide range of vehicle classes to support conceptual design. This is accomplished by performing exact, analytic integrations of the Newtonian pressure coefficient over the unshadowed surface of the vehicle where possible and analytically approximating the remaining terms. Comparisons with a panel method validate the analytic solutions formed for arbitrary bodies of revolution with profiles described by second-, third-, or fourth-order Bezier curves as well as non-axisymmetric geometries described by constrained second-order Bezier surfaces. The computational and design advantages provided by the analytic relations enable the rapid design of vehicle shape within conceptual studies in manner that is not possible with traditional panel methods.

Nomenclature

$\hat{\mathbf{n}}_{\mathbf{in}}$	inward normal vector	C_p	pressure coefficient
$\mathbf{B}$	control node location, m	C_S	side force coefficient
$\mathbf{P}$	Bezier function, m	n	order of Bezier curve
$\mathbf{r}$	position of differential surface element, m	N_u	number of discrete elements along u
A_{ref}	reference area, m^2	N_v	number of discrete elements along v
C_A	axial force coefficient	p_∞	freestream pressure, Pa
C_l	roll moment coefficient	u	arclength, surface parametrization variable
C_m	pitch moment coefficient	v	surface parametrization variable
C_N	normal force coefficient	V_∞	freestream velocity magnitude, m/s
C_n	yaw moment coefficient		
ρ_∞	freestream density, kg/m^3	θ	inclination angle, rad

I. Introduction and Motivation

Traditionally, multidisciplinary hypersonic conceptual design is performed in a sequential, iterative design environment comprised of independently developed disciplinary analyses. In this environment, design variables are separately chosen within each discipline. As a result, the interaction among cross-discipline variables is segregated, limiting the use of fast, specialized optimization methods in favor of slower, more generalized methods. Typically, the early phases of conceptual hypersonic design are executed to identify the type and configuration of the vehicle as well as the corresponding envelope of trajectory capability. With this consideration, hypersonic vehicle capability is generally identified through iteration among vehicle shape, aerodynamic performance, and trajectory optimization routines as shown in Fig. 1. This sequential, iterative process is the result of a fundamental segregation between vehicle shape and trajectory optimization routines that results from the characterization of aerodynamic performance for each vehicle shape using large

*Assistant Professor, School of Aeronautics and Astronautics, AIAA Member.

aerodynamic tables that are a function of vehicle orientation and flight conditions. As a result, this numerical relationship has also segregated advancements in vehicle shape design from advancements in trajectory optimization.

The hypersonic aerodynamics of vehicles are often modeled during conceptual design using Newtonian flow theory.[1,2] This theory assumes that when a particle (traveling in rectilinear motion) strikes the surface of a body, all of the momentum normal to the surface would be lost and all momentum tangential to the surface would be conserved as shown in Fig. 2. Consequently, the pressure exerted by the fluid on the surface of a body is assumed to be solely originating from this loss of momentum normal to the surface. Under these assumptions, the nondimensional pressure coefficient, C_p, at any point on the surface of a body can be obtained from the Newtonian sine-squared relation shown in Eq. (1). Furthermore, the pressure exerted by the fluid on any portion of the surface not directly exposed to the flow, denoted as the shadowed region of the body, is assumed to be equivalent to the freestream pressure in which the motion of the fluid does not influence the pressure in this region. Consequently, $C_p = 0$ throughout the shadowed region as shown in Fig. 3. While this theory is only accurate within continuum flow at high speeds, this flight condition is often achieved during trajectory segments with high dynamic pressure. As such, Newtonian flow theory is a reasonable approximation during meaningful trajectory segments in which the vehicle has the greatest capability to alter its motion. The aerodynamic force and moment coefficients are obtained by integrating the pressure coefficient over the unshadowed surface of the vehicle.

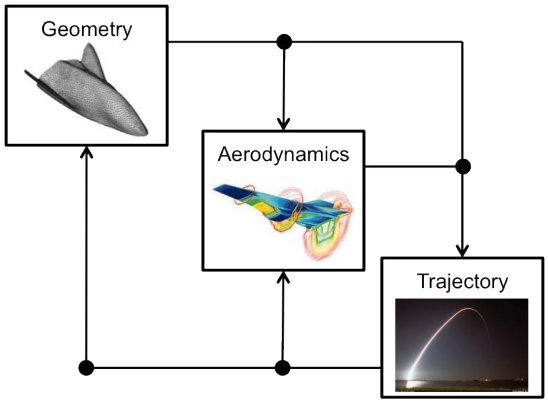

Figure 1: Example design structure matrix for hypersonic performance characterization.

$$C_p = \frac{p - p_\infty}{\frac{1}{2}\rho_\infty V_\infty^2} = 2\sin^2\theta \tag{1}$$

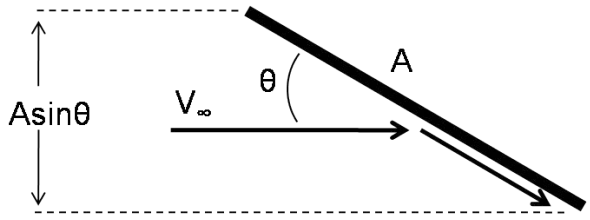

Figure 2: Momentum transfer of particle on inclined surface.[2]

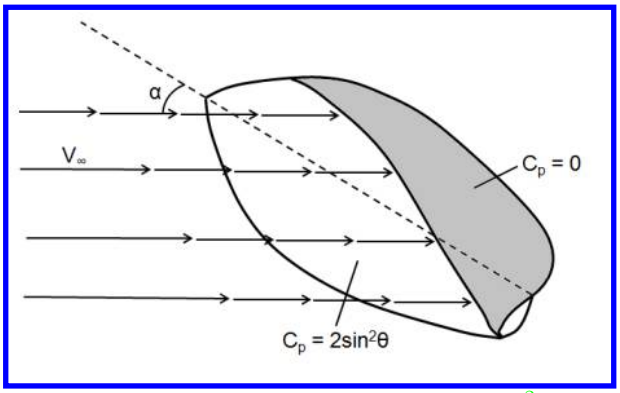

Figure 3: Example of shadowed body.[2]

Traditionally, this integration is performed numerically through the use of ring methods[3,4,5] or panel methods such as those included within the Configuration Based Aerodynamics (CBAERO) tool[6] and the Aerodynamic Preliminary Analysis System (APAS).[7,8,9] In this approach, the geometry of the vehicle is approximated as a series of small flat plates, and the numerical integration is performed repeatedly across a range of orientations of interest to generate large aerodynamic tables. This procedure is repeated for each vehicle shape analyzed during conceptual design, and the advent of the digital computer has resulted in widespread adoption of panel methods.[10,11] However, the analytic description of the flowfield (Eq. (1)) and recent advances in symbolic tools such as Mathematica[12] enable the surface integration to be performed analytically. In prior work, analytic force and moment coefficients were constructed for a wide range of basic shapes, including conical frustums, spherical segments, flat plates, and cylindrical segments.[13] Additional

relations for quadratic- and parabolic-based shapes were also constructed through the use of boundary-volume techniques and other transformations.[14,15,16] Since many hypersonic vehicles of interest can be constructed through the superposition of these basic shapes as shown in Fig. 4,[17,18,19,20,21,22] the hypersonic aerodynamics of these systems can also be expressed analytically through the appropriate combination of the analytic aerodynamic relations.

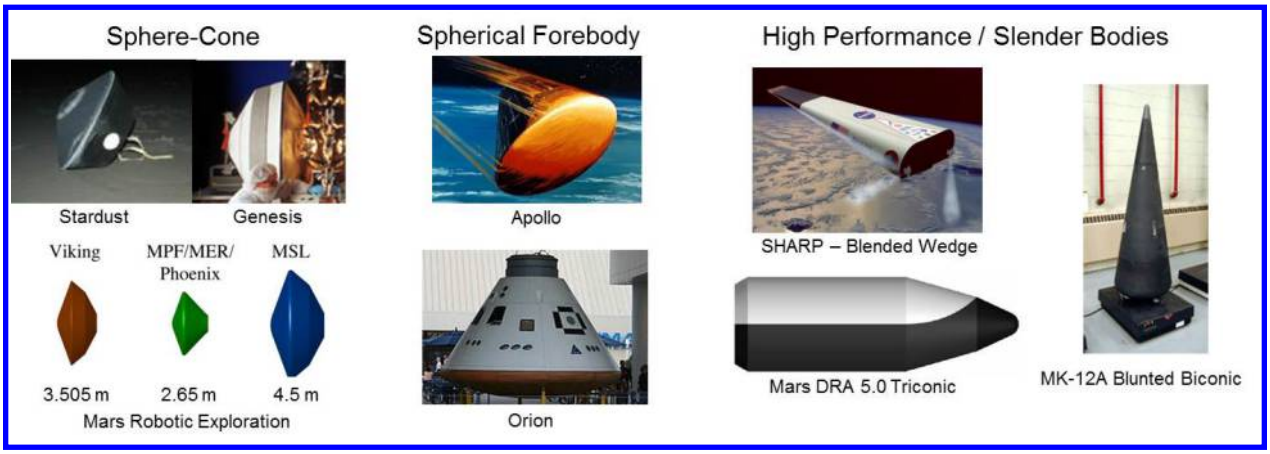

Figure 4: Example vehicles with analytic geometries.

The analytic relations have been shown to be approximately three orders of magnitude faster than the construction and evaluation of tables using CBAERO.[14] This speedup could be capitalized within traditional, segregated design environments by replacing tables with the analytic relations. More importantly, these relations provide an analytic mapping between vehicle shape and trajectory performance. Since the analytic relations are generically parametrized by vehicle shape parameters and are applicable across all corresponding geometries, vehicle shape parameters can be directly incorporated into the equations of motion as shown in Fig. 5 for an example sphere cone with nose radius r_n, cone half angle δ_1, and base diameter d. In this example, the vehicle geometry is assumed to be fixed during flight, but this framework could also be used with varying shape parameters as a result of ablation or configuration changes during flight. Note that in this approach, the vehicle shape parameters are combined with trajectory states in a fully coupled manner that eliminates the iteration between vehicle shape and trajectory that previously existed due to the intermediate aerodynamic tables. This fully coupled system enables rapid indirect trajectory optimization principles to be extended to also include vehicle shape to perform rapid simultaneous hypersonic aerodynamic and trajectory optimization in a manner that is not possible within traditional segregated design environments.[14,23,24]

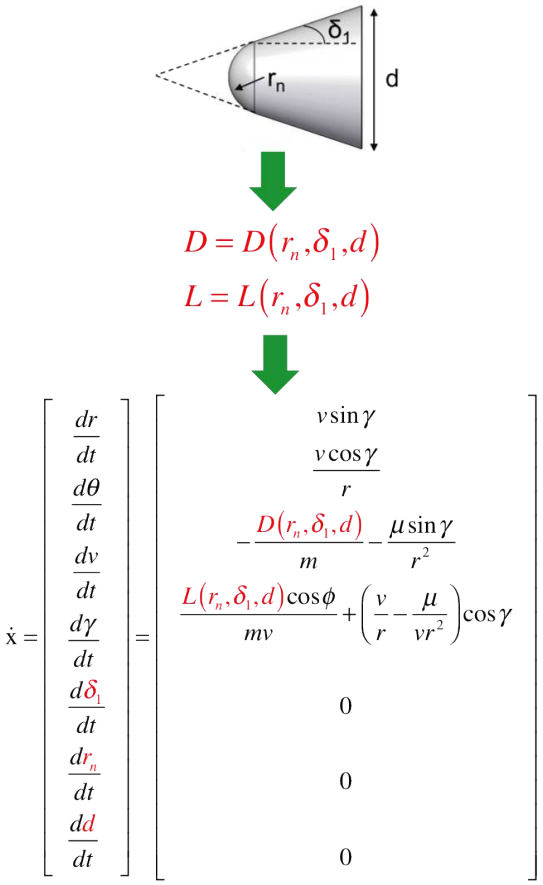

Figure 5: Coupled hypersonic aerodynamic and trajectory system.

While the previously developed analytic relations enable the rapid design of various hypersonic systems of interest, the range of geometries that have exact, analytic solutions are limited, and as a result, prevents the adoption of these computationally efficient relations into conceptual design studies. For many complex

shapes, no exact analytic force or moment solution can be constructed, and this is a consequence of the fundamental challenges that exist when performing complex integrations symbolically.[14,15,16] To expand the current analytic aerodynamic database to also include general vehicle configurations, hybrid exact-approximate analytic solutions are constructed for Bezier curves of revolution and Bezier surfaces. Note that these relations are generically parametrized by an appropriate set of control nodes. As such, the analytic relations developed in this investigation are applicable across all configurations that can be represented by Bezier curves of revolution and Bezier surfaces. This is a major advantage over panel methods that must be executed each time the shape of the vehicle changes. The current analytic aerodynamic database, that includes the analytic relations derived in this investigation, can be downloaded from the following embedded file when viewed in Adobe Acrobat (aerodynamicsDatabase.zipREMOVEME)[a]. The enclosed Matlab routines should be referenced for the contents of the analytic expressions.

II. Hybrid Exact-Approximate Analytic Solutions

Exact, analytic relations are only constructed if every expression within the integration process has a known integral. However, hybrid exact-approximate solutions can be constructed for general vehicle configurations that are also fully analytic. To support the rapid simultaneous design environment shown in Fig. 5, each analytic aerodynamic expression must be valid across the entire range of both shadowed and unshadowed orientations. This requirement prevents the construction of fully approximate solutions that span the entire surface of the vehicle. As an example, consider a generic body with a surface parametrization in u and v as shown in Eq. (2). With this surface parametrization, the inward unit normal, $\hat{\mathbf{n}}_{\mathbf{in}}$, can be formulated, and the pressure coefficient can be computed using Eqs. (1), (3), and (4).

$$\mathbf{r} = [f(u,v) \quad g(u,v) \quad h(u,v)]^T \tag{2}$$

$$\hat{\mathbf{n}}_{\mathbf{in}} = \frac{\mathbf{r_u} \times \mathbf{r_v}}{\| \mathbf{r_u} \times \mathbf{r_v} \|} \tag{3}$$

$$\sin(\theta) = \hat{\mathbf{V}}_{\infty}^{T} \hat{\mathbf{n}}_{\mathbf{in}} \tag{4}$$

The integration of the pressure coefficient over the surface of the vehicle could be approximated as shown in Eq. (5) for a force coefficient in the x-direction, where S denotes the unshadowed surface of the vehicle and the differential area is computed using Eq. (6). This procedure is analogous to the surface integration performed by a panel method. However, the approximation shown in Eq. (5) is performed directly on the aerodynamics of vehicle as opposed to the shape of the vehicle, providing a fully analytic approximation. Note that the finite sum in at least one variable changes as the orientation of the vehicle changes to account for the moving shadow boundary. As a result, the number of terms in the finite summation would vary or the manner in which the surface quadrature is calculated would be altered due to the shift in node locations for each shadowed orientation, preventing the adoption of this analytic approximation within the design environment shown in Fig. 5. Alternatively, if one of the surface integrations can be performed analytically to allow for an analytic substitution of the shadow boundary (shown in Eq. (7)), then a single hybrid exact-approximate analytic solution can be formulated that is valid across all shadowed and unshadowed orientations. This feature requires the shadow boundary to be fully determined by v as a function of u, allowing the approximation to be performed along u chosen to be constant regardless of the shadow boundary. This form enables the complex and changing shadow boundary to be incorporated analytically within the hybrid solutions. While a Riemann sum analogous to the calculations performed within a panel method is shown in this example, any quadrature scheme could be used. For efficiency, a Legendre-Gauss-Lobatto quadrature scheme is used in this investigation. Since the complexity of the integrated terms increases with the number of integration performed, this single exact integration procedure provides the greatest opportunity to construct analytic, hybrid exact-approximate solutions for general vehicle configurations. As

[a]Prior to unzipping the file, the 'REMOVEME' portion of the file extension must be removed.

such, the extent of general vehicle configurations that have analytic solutions of this form is investigated.

$$C_X = \frac{1}{A_{ref}} \iint_S C_p \ \hat{\mathbf{n}}_{\mathbf{in}}^T \hat{\mathbf{x}} \ \mathrm{d}A \approx \frac{1}{A_{ref}} \sum_{i=0}^{N_u} \sum_{j=0}^{N_v} C_{p,\{i,j\}} \ \mathbf{n}_{\mathbf{in},\{\mathbf{i},\mathbf{j}\}}{}^T \hat{\mathbf{x}} \ \Delta A_{\{i,j\}} \tag{5}$$

$$\mathrm{d}A = \| \ \mathbf{n} \ \| = \| \ \mathbf{r}_u \times \mathbf{r}_v \ \| \tag{6}$$

$$C_X = \frac{1}{A_{ref}} \int_{u_1}^{u_2} \int_{v_1(u)}^{v_2(u)} C_p \ \hat{\mathbf{n}}_{\mathbf{in}}^T \hat{\mathbf{x}} \ \mathrm{d}A = \frac{1}{A_{ref}} \int_{u_1}^{u_2} F(u) \ \mathrm{d}u \approx \frac{1}{A_{ref}} \sum_{i=0}^{N_u} F(u) \ \Delta u \tag{7}$$

Unlike panel methods, the hybrid exact-approximate relations directly approximate the final aerodynamic result, and the error of this result can be directly controlled to obtain a desired accuracy. Alternatively, panel methods approximate vehicle shape to a certain level of accuracy, and the designer usually does not know *a priori* how this approximation translates to the accuracy of the aerodynamic coefficients. Consequently, multiple meshes of varying resolutions must be evaluated until convergence of the aerodynamic coefficients is observed.

II.A. Bezier Curves of Revolution

Many methods from computer-aided design exist to describe general shapes. As an initial step in this direction, analytic force and moment coefficients have been developed for Bezier curves of revolution with various orders. While high-order analytic relations have been obtained, the resulting expressions are lengthy, limiting the computational efficiency of this approach. While the efficiency of these higher-order solutions could likely be improved with symbolic manipulation (*e.g.*, performing repeated calculations once and storing the result in memory), solutions for second-, third-, and fourth-order Bezier curves of revolution are included in this report. Note that these relations account for both shadowed and unshadowed angles of attack. Since these geometries are axisymmetric, the resulting analytic relations can be evaluated at total angles of attack and rotated to the proper wind frame to also account for nonzero sideslip angles (illustrated within the enclosed database).

The geometry of a Bezier curve is parametrized by a nondimensional arclength, u, as shown in Eqs. (8)-(10) where $0 \leq u \leq 1$.[25] The location of the i^{th} control node is specified by the vector $\mathbf{B_i}$, and the order of the Bezier curve is specified by n. The control nodes specify a control polygon inside which the Bezier curve must reside. While the analytic relations are generically parametrized to control node locations, the use of Newtonian flow theory requires the evaluated shapes to be convex with a nondecreasing radius along the axis of the vehicle. Example second-, third-, and fourth-order Bezier curves, along with their corresponding control node locations and control polygons, are shown in Fig. 6. As expected, each Bezier curve resides inside the control polygon and is connected to the initial and final control nodes in a tangential manner to the control polygon. While the addition of control nodes in higher-order solutions would provide greater flexibility in describing the shape of the vehicle, it is apparent that substantially curved profiles can be achieved with a fourth-order Bezier curve. As such, the increase in computational resources beyond fourth-order solutions is likely not necessary during conceptual design. In fact, many conceptual design studies could likely be accomplished with a low-order Bezier curve. To determine if low-order curves are sufficient

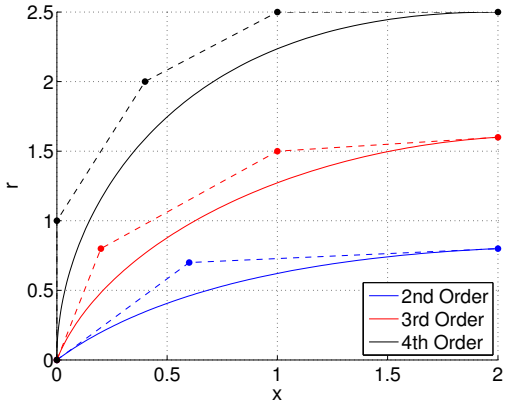

Figure 6: Bezier curves with control nodes and control polygons.

for a particular study, optimal solutions can be investigated with higher-order solutions until convergence in solution shape is observed.

$$\mathbf{P}(u) = \sum_{i=0}^{n} \mathbf{B_i}\ J_{n,i}(u) \tag{8}$$

$$J_{n,i}(u) = \binom{n}{i} u^i (1-u)^{n-i} \tag{9}$$

$$\binom{n}{i} = \frac{n!}{i!(n-i)!} \tag{10}$$

The surface of a Bezier curve of revolution is most naturally parametrized along u (the nondimensional arclength along the Bezier curve) and v (the revolution angle of the Bezier curve) as described by Eq. (11), where $x(u)$ and $r(u)$ are determined by expressions resulting from Eq. (8). In the derivation of these relations, the shadow boundary (where $C_p = 0$) is fully incorporated for all angles of attack and sideslip by noting that the limits in the revolution angle, v, are calculated from inverse trigonometric functions. When the vehicle is fully exposed to the flow, the revolution angle inherits a nonzero imaginary component. Thus, by evaluating the real component of this expression, valid limits in revolution angle are constructed that simultaneously account for both shadowed and unshadowed angles of attack and sideslip. This property is essential in the construction of invariant analytic expressions to support the coupled, multidisciplinary design environment shown in Fig. 5. The analytic solutions to various second-order Bezier curves shown in Fig. 7 are validated using a separately developed panel method as shown in Figs. 8-10. As shown, both sets of results are in excellent agreement. Note that each force and moment coefficient as well as each stability derivative is calculated from a single corresponding analytic solution. As such, the invariant set of analytic solutions is used to calculate all of the analytic aerodynamic data shown in Figs. 8-10. While the analytic relations could be used to rapidly construct aerodynamic tables to support traditional conceptual design environments, the analytic solutions also enable these shapes to be included within the rapid, simultaneous optimization framework as described in Section I.

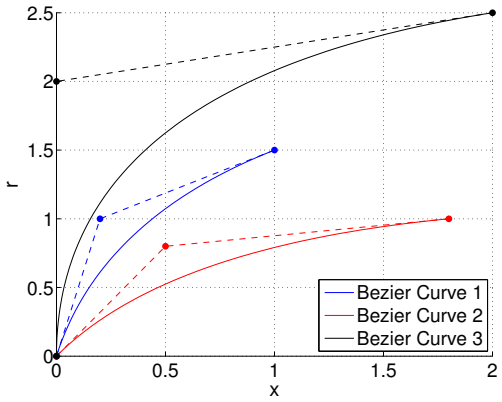

Figure 7: Validated 2nd order Bezier curves.

$$r = [x(u) \quad r(u)\cos(v) \quad -r(u)\sin(v)]^T \tag{11}$$

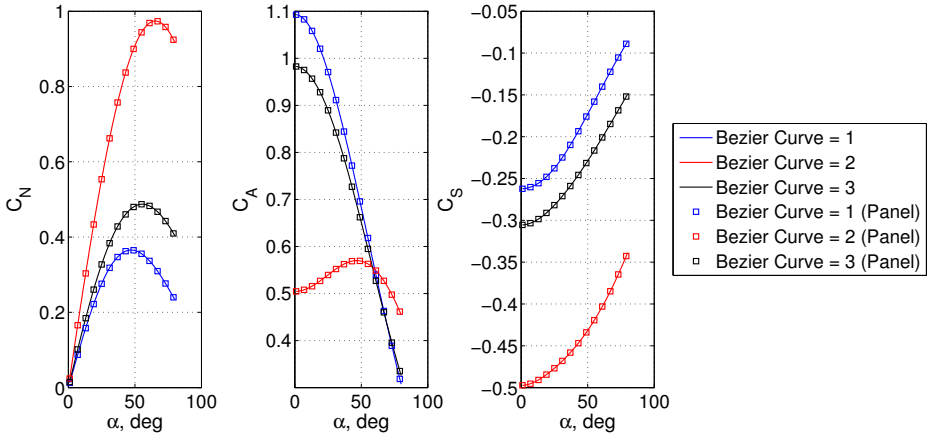

Figure 8: Validated forces for 2nd order Bezier curves ($\beta = 20^o$).

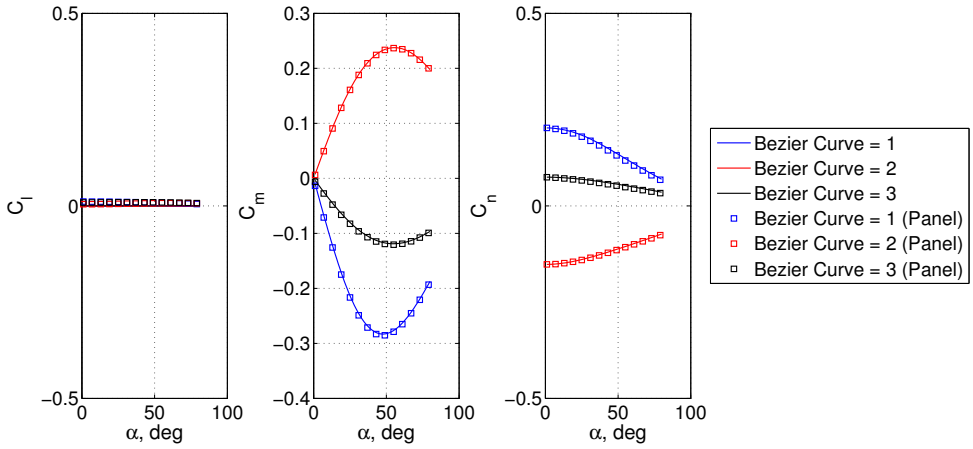

Figure 9: Validated moments for 2nd order Bezier curves ($\beta = 20^o$).

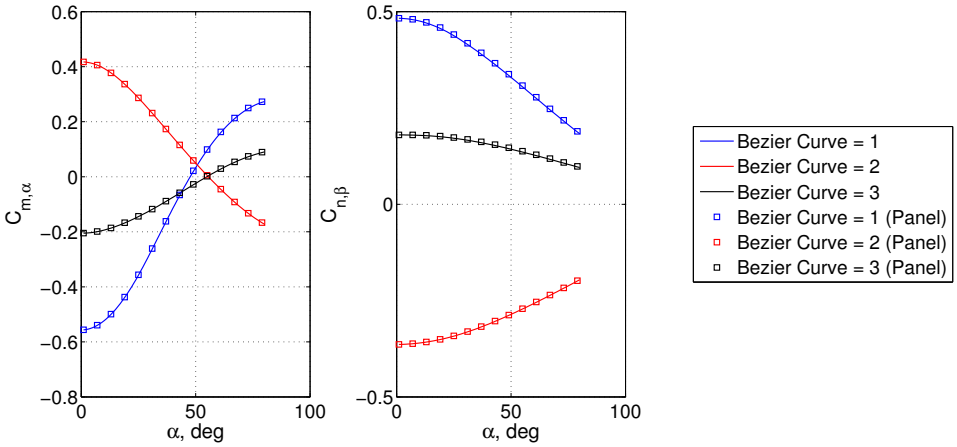

Figure 10: Validated stability derivatives for 2nd order Bezier curves ($\beta = 20^o$).

The third- and fourth-order Bezier curves shown in Figs. 11 and 12 are also validated using the panel method as shown in Figs. 13-16. As illustrated, excellent agreement exists for both the force and moment coefficients. Note that a small discrepancy in roll moment coefficient (C_l) is observed due to the full approximation by the panel method. For axisymmetric bodies, the roll moment coefficient should be zero, and this result is obtained from the analytic relations. It is important to note that the stability derivatives of these higher-order curves are lengthy and not included. While the use of symbolic manipulation may enable the construction of efficient stability derivative expressions that are reasonably short in length, it may also be better to compute these derivatives numerically using a finite difference or complex step method on the validated analytic moment expressions. Figs. 11 and 12 illustrate that these higher order curves provide additional flexibility likely required to represent a range of blunt configurations. To achieve a fully blunt configuration, two control nodes must reside on the vertical axis as shown by the third Bezier curve in each figure. As an alternative, the front portion of sharp Bezier curves of revolution could be replaced with an appropriate spherical segment (of which analytic relations have already been developed),[13] enabling the use of low-order Bezier cures for blunt configurations. Finally, as the bluntness of the vehicle increases, the corresponding aerodynamic coefficients may change dramatically as shown in Figs. 13 and 14. The analytic relations are capable of capturing these large changes within each invariant expression.

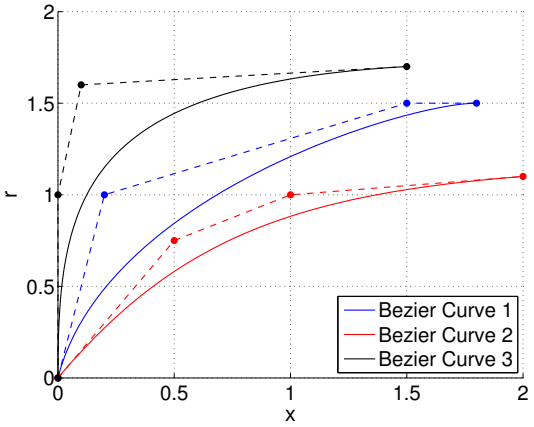

Figure 11: Validated 3rd order Bezier curves.

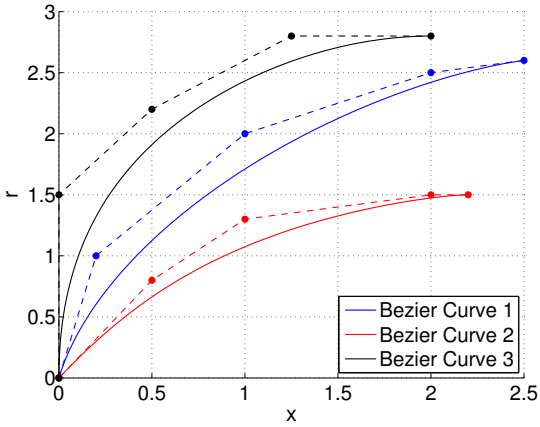

Figure 12: Validated 4th order Bezier curves.

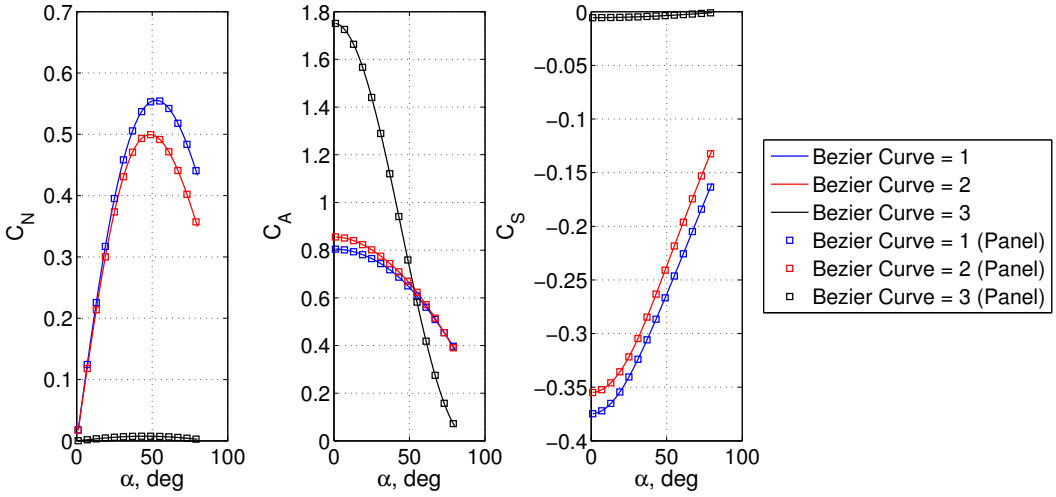

Figure 13: Validated forces for 3rd order Bezier curves ($\beta = 20^o$).

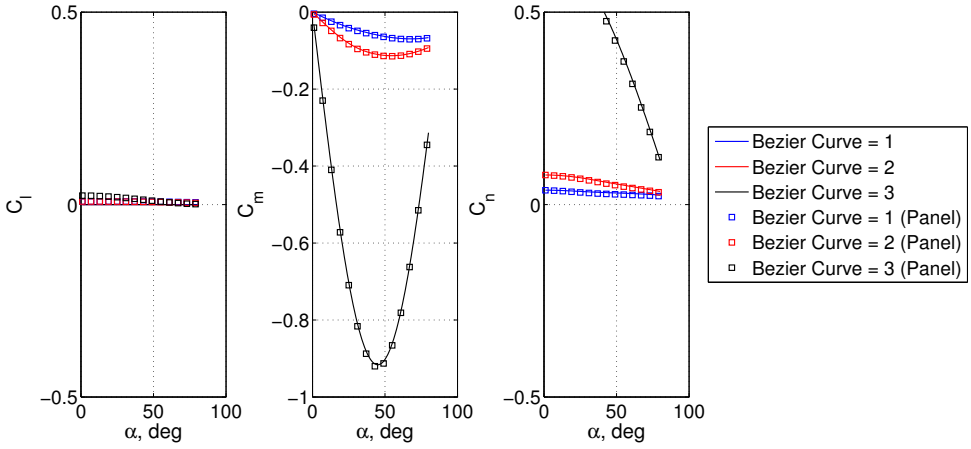

Figure 14: Validated moments for 3rd order Bezier curves ($\beta = 20^o$).

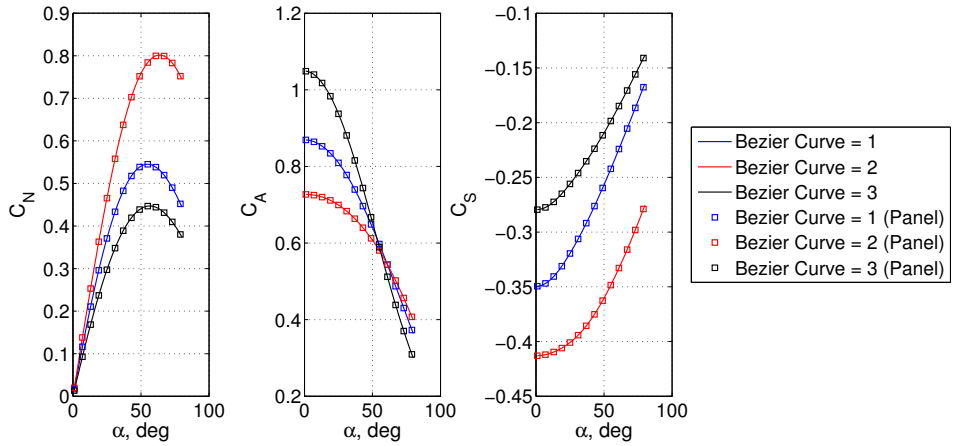

Figure 15: Validated forces for 4$^{\text{th}}$ order Bezier curves ($\beta = 20^o$).

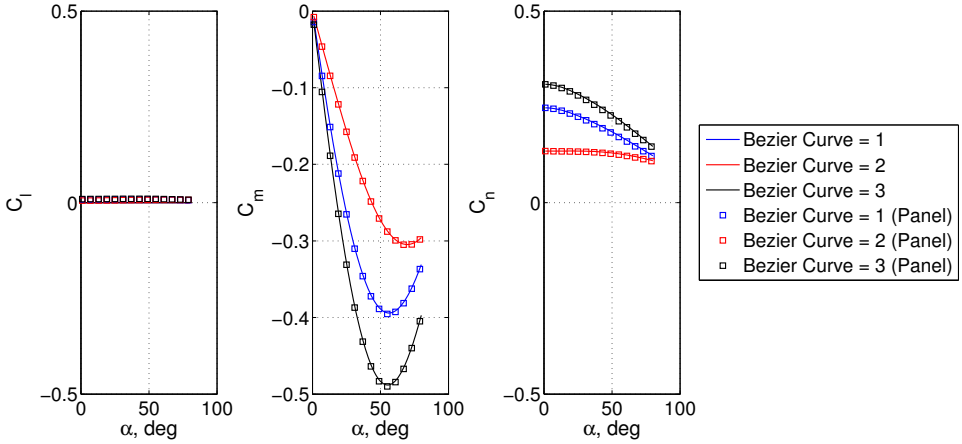

Figure 16: Validated moments for 4$^{\text{th}}$ order Bezier curves ($\beta = 20^o$).

II.B. Bezier Surfaces

While the prior analytic solutions enable the rapid design and analysis of arbitrary bodies of revolution, future missions may require vehicle performance that is outside of the axisymmetric envelope. As such, the construction of hybrid exact-approximate analytic solutions for non-axisymmetric bodies is investigated. As an extension to Bezier curves, the geometry of these arbitrary bodies is described using Bezier surfaces. The geometry of a Bezier surface is constructed by Eq. (12), where $\mathbf{B_{i,j}}$ describes the three dimensional control node locations. While the construction of analytic solutions to high-order Bezier surfaces is ongoing, preliminary analysis has shown that hybrid exact-approximate analytic solutions can be constructed for a specific set of second-order Bezier surfaces where $n = m = 2$. The analytic relations contained in the attached database correspond to second-order surfaces with edge control nodes fixed at locations within the same plane. An example of this is shown in Fig. 17 in which the eight edge control nodes reside along the edges of a square. To construct various Bezier surfaces, the central control node is moved as desired in any direction. Note that if the central control node was placed in the center of the square, then the Bezier surface would also take the shape of the square. As the central control node is moved away from this location, the Bezier surface is stretched while remaining anchored along the edges. As shown by the front view in Fig. 18, this central control node can be moved in any manner to construct non-axisymmetric configurations.

$$\mathbf{P}(u,v) = \sum_{i=0}^{n} \sum_{j=0}^{m} \mathbf{B_{i,j}} \; J_{n,i}(u) \; J_{m,j}(v) \tag{12}$$

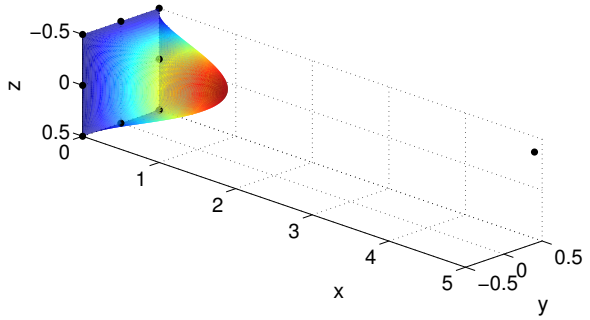

Figure 17: Angled view of validated 2nd order Bezier surface.

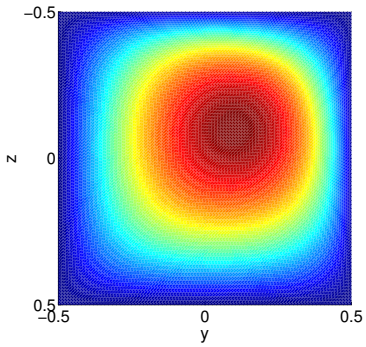

Figure 18: Front view of validated 2nd order Bezier surface.

As with the hybrid exact-approximate analytic solutions constructed for Bezier curves of revolution, hybrid solutions are constructed by analytically integrating with respect to v and substituting an analytic expression for the shadow boundary. Unlike Bezier curves of revolution, the limits in v provided by the shadow boundary are not derived from inverse trigonometric functions. Instead, the shadowed region of Bezier surfaces is highly complex, but a single expression for the shadow boundary must be created such that an invariant set of analytic aerodynamic relations are created. When the surface is completely unshadowed, $0 \leq v \leq 1$ where $v = 0$ at the most positive z-locations and $v = 1$ at the most negative z-locations. However, solution to the shadow boundary where $C_p = 0$ will result in limits in v that exceed 1 for unshadowed orientations and will also result in limits in v that have a nonzero complex component for shadowed orientations. To accommodate both shadowed and unshadowed orientations with an invariant expression, the upper limit in v is transformed through a sequence of real and imaginary component calculations as well as trigonometric transformations as shown in Eq. (13), where $f(u)$ is calculated from $v = f(u)$ along the shadow boundary. Note that the expression $v = f(u)$ along the shadow boundary is complex, and this transformation is not obvious when analyzing the result. Instead, this relationship was constructed after numerically evaluating the properties of $f(u)$ along various portions of the shadow boundary.

$$v_{\text{upper}} = \sin(\Re(\arcsin(\Re(f(u)) - \Im(f(u))))) \tag{13}$$

The non-axisymmetric Bezier surfaces described by the central control node locations shown in Table 1 are validated using the panel method as shown in Figs. 19 and 20. Note that this validation is conducted at a zero sideslip, and the analytic relations currently do not account for nonzero sideslip angles. Due to the lack of symmetry, a side force, roll moment, and yaw moment is generated at zero sideslip angles. While these particular configurations would likely not be used for these reasons (the asymmetry would likely only reside along the y-axis), the validated solutions illustrate that relatively complex non-axisymmetric analytic solutions can be constructed. While excellent agreement exists in the force coefficients, a minor discrepancy is observed in the moment coefficients. This illustrates the fully approximate nature of panel methods in which the shape of the vehicle is approximated using small flat plates. For slender vehicles with complex shadow boundaries, the paneled integration demonstrates a slowly converging solution to the analytic result. This illustrates a challenge of using panel methods for high-performance, slender configurations. Since the mapping of vehicle shape accuracy to aerodynamic coefficient accuracy is not known *a priori*, multiple paneled vehicles of various accuracies are required until convergence of the aerodynamic relations is observed. Since the hybrid relations only require a quadrature rule along one direction, u, a highly accurate solution can be constructed with a relatively few number of efficient quadrature locations. In this work, a sufficient number of Legendre-Gauss-Lobatto points (30) was chosen to ensure convergence of the numerical hybrid solutions across all geometries investigated.

Table 1: Central node validation locations.

B_x	B_y	B_z
5.0	0.4	-0.4
10.0	-0.3	-0.2

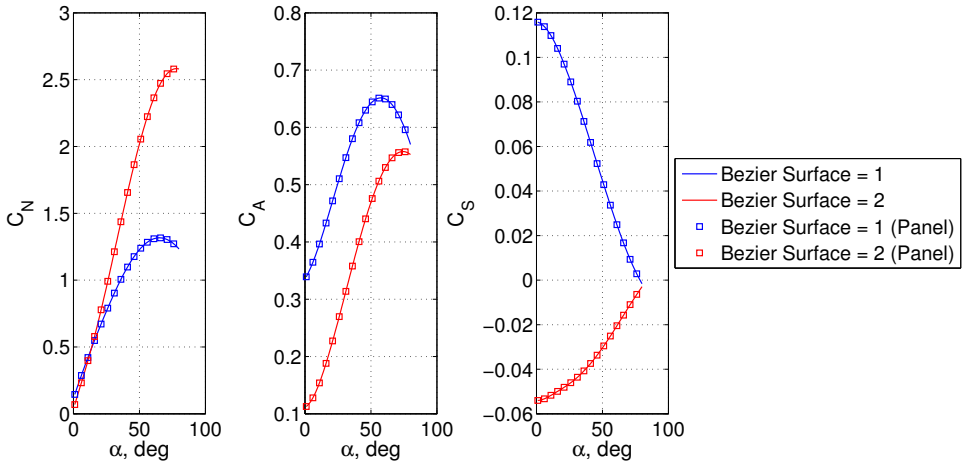

Figure 19: Validated forces for 2nd order Bezier surface ($\beta = 0^o$).

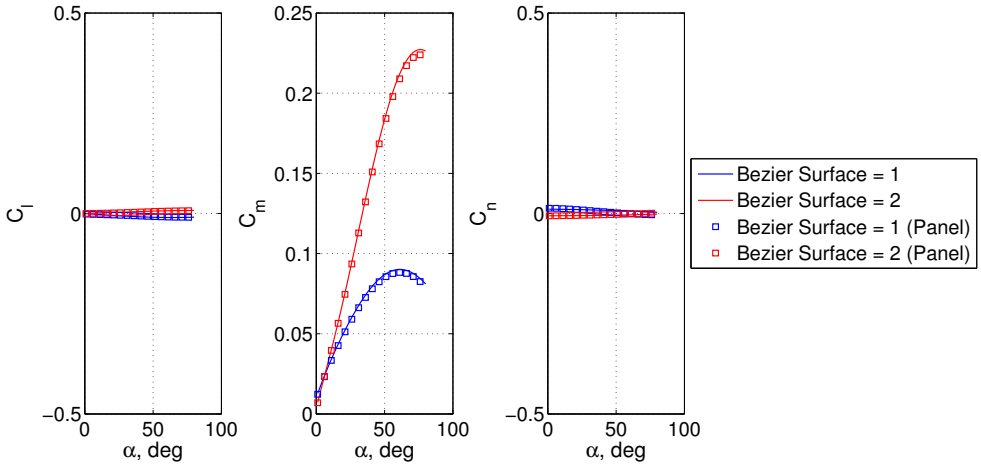

Figure 20: Validated moments for 2nd order Bezier surface ($\beta = 0^o$).

III. Computational Performance of the Hybrid Relations

To illustrate the computational speed of the hybrid exact-approximate analytic relations obtained in this investigation, the average compute time of evaluating each solution during the validation process on a dual-core 2 GHz modern laptop is listed in Table 2. Note that these times were calculated from the evaluation of Matlab functions as well as functions autocoded to C. While improvement of approximately one to two orders of magnitude is generally obtained by autocoding these analytic results into C, the lengthy expressions of fourth-order Bezier curves prevented this conversion.

Table 2: Execution speed comparisons.

Geometry	Mean Compute Time (Autocoded)
2nd Order Bezier Curve	0.195 s (0.00185 s)
3rd Order Bezier Curve	0.329 s (0.0281 s)
4th Order Bezier Curve	0.849 s (-)
2nd Order Bezier Surface	0.257 s (0.0413 s)

The fast execution of the Bezier curves of revolution suggests that these relations could likely replace panel methods for all studies of bodies of revolution. Additionally, these results indicate that the hybrid exact-approximation solutions, which require an analytic approximation for one integration, are efficient for both axisymmetric and non-axisymmetric solutions. As such, these results indicate that further investigations into non-axisymmetric solutions will likely be worthwhile. While the rapid execution would enable these methods to replace panel methods to generate large aerodynamics tables of force and moment coefficients,

the fast compute times indicate that these general expressions could also be efficiently incorporated within the mathematically coupled, multidisciplinary design environment described in Section I.

IV. Future Work

This investigation demonstrated that efficient hybrid exact-approximate analytic solutions can be constructed for general vehicle configurations. However, as illustrated in the enclosed database, the resulting analytic expressions are lengthy, and many redundant calculated are embedded within the various relations. For example, investigation of the force and moment solutions to the second-order Bezier curve of revolution indicate that there are many common calculations such as those listed in Table 3. To improve execution speed, repeated calculations such as these should be calculated once, stored in memory, and referenced throughout the analytic expressions. As such, a symbolic optimization engine should be created that is capable of analyzing the lengthy analytic expressions to identify common terms and perform the corresponding symbolic substitutions. Note that this procedure is more challenging than may otherwise be expected. As a simple example, if the term $2u^2$ is repeated throughout an expression, then it is challenging to differentiate this term with the term $2u^{20}$. As a result, a detailed analysis of nearby characters must be performed to ensure that the symbolic substitutions do not change the overall calculation. After these substitutions are made, then it may be possible to autocode higher-order solutions, including those of the fourth-order Bezier curve of revolution. To further enhance execution speed, a detailed quadrature analysis should be conducted to determine the appropriate number of terms that may be best suited for each particular class of shapes. Note that since a highly efficient quadrature scheme was used in this investigation, the benefits of this analysis will be secondary to the aforementioned symbolic optimization.

Table 3: Common 2^{nd} order Bezier curve of revolution expressions.

Repeated Expression
$b_{1x}b_{2x}(-1+2u+3u^2-4u^3)$
$2b_{1x}^2u(1-3u+2u^2)$
$b_{1y}b_{2y}(3-4u)u$
$b_{2x}^2(-1+u^2)$
$b_{1y}^2(2-6u+4u^2)$
$(b_{2x}^2+b_{2y}^2)u^2$
$2b_{1x}b_{2x}(1-2u)u$
$2b_{1y}b_{2y}(1-2u)u$
$b_{1x}^2(1-2u)^2$
$2b_{1y}(-1+u)$
$8b_{1y}^2u^3(-2b_{1y}(-1+u)+b_{2y}u)$
$b_{1y}b_{2y}u(-1+2u)$

While the efficiency of existing analytic relations should be improved as much as possible, the limit of non-axisymmetric hybrid exact-approximate analytic solutions should be further investigated. As shown in Section II.B, limited solutions for 2^{nd} order Bezier surfaces have been constructed for anchored edge control nodes. However, when these anchored values are replaced with general constants, the current analytic integration procedure fails. Since the constant anchored values are replaced with an unspecified constant, solutions to this more general representation of the Bezier surface should exist. However, the complexities associated with the analytic integration process (*e.g.*, real vs. complex domain analysis, assumptions on the relative arrangement of the node locations, etc.) have likely precluded the discovery of these more general solutions. Further investigation of these considerations may yield new solutions.

The major challenge associated with this investigation is that many expressions have no known integral, preventing the construction of analytic solutions. To avoid these integration challenges, the inverse aerodynamic problem should be studied in detail. In this potentially useful approach, the analytic aerodynamics would be specified *a priori*, and the shape of the vehicle could be estimated via differentiation of these analytic relations. Since differentiation is a relatively straightforward process, this approach would not be subject to the integration challenges that are addressed in this investigation. As solutions to new configurations are explored, special consideration should be given to emerging technologies such as morphing or flexible structures. For example, analytic relations for inflatable aerodynamic decelerators would enable the real-time modeling of shape change during trajectory propagation. As such, these relations could be used to improve the hypersonic modeling of passively flexible systems or to support targeting studies of actively controlled systems.

V. Summary

In this investigation, hybrid exact-approximate analytic aerodynamic relations are constructed for general vehicle configurations based on Newtonian flow theory. These relations serve to expand on the prior analytic aerodynamic database that consisted of solutions to specific shapes such as spherical segments, conical

frustums, etc. Solutions to second-, third-, and fourth-order Bezier curves of revolution were constructed by performing the first surface integration analytically and subsequently incorporating the analytic shadow boundary into this result. Due to the complexity of the resulting expression, the final surface integration is approximated analytically. Since the unshadowed surface limits have already been incorporated into the solution, this final integration is performed in a manner that is independent of the orientation of the vehicle. As such, solutions in both force and moment coefficients are created that account for both shadowed and unshadowed orientations. Since these analytic solutions are invariant, they can be incorporated into the mathematically coupled multidisciplinary design environment as described in Section I. Additionally, the majority of axisymmetric vehicles of interest can likely be represented by these Bezier curves of revolution, and as a result, conceptual design studies of axisymmetric vehicles would likely not require the use of panel methods. To further expand the domain of hybrid exact-approximate analytic relations, solutions to constrained second-order Bezier surfaces were also constructed for a zero sideslip. These solutions require the outer nodes to be anchored within the same plane, allowing the central node to be arbitrarily located to construct various non-axisymmetric geometries. Comparisons with an independently developed panel method validate the analytic solutions derived for both Bezier curves of revolution and Bezier surfaces. Average compute times of a fraction of a second illustrate the computational efficiency of the hybrid exact-approximate analytic relations to support conceptual hypersonic design studies.

References

[1]Newton, I., *Principia - Motte's Translation Revised*, University of California Press, 1946.

[2]Anderson, J. D., *Hypersonic and High Temperature Gas Dynamics*, AIAA, 1989.

[3]Rainey, R. W., "Working Charts for Rapid Prediction of Force and Pressure Coefficients on Arbitrary Bodies of Revolution by Use of Newtonian Concepts," *NASA TN D-176*, 1959.

[4]Margolis, K., "Theoretical Evaluation of the Pressures, Forces, and Moments at Hypersonic Speeds Acting on Arbitrary Bodies of Revolution Undergoing Separate and Combined Angle-of-Attack and Pitching Motions," *NASA TN D-652*, 1961.

[5]Grimminger, G., Williams, E. P., and Young, G. B. W., "Lift on Inclined Bodies of Revolution in Hypersonic Flow," *Journal of the Aeronautical Sciences*, Vol. 17, No. 11, 1950.

[6]Kinney, D. J., "Aero-Thermodynamics for Conceptual Design," AIAA-2004-31-962, *42nd AIAA Aerospace Sciences Meeting and Exhibit*, Reno, NV, 5-8 Jan. 2004.

[7]Bonner, E., Clever, W., and Dunn, K., "Aerodynamic Preliminary Analysis System II: Part I Theory," *NASA-CR-165627*, Apr. 1981.

[8]Smyth, D. N. and Loo, H. C., "Analysis of Static Pressure Data from 1/12-scale Model of the YF-12A. Volume 3: The MARK IVS Supersonic-Hypersonic Arbitrary Body Program, User's Manual," *NASA-CR-151940*, Oct. 1981.

[9]Cunningham, M., "Hypersonic Aerodynamics for an Entry Research Vehicle," *Journal of Spacecraft and Rockets*, Vol. 24, No. 2, 1987.

[10]Theisinger, J. E. and Braun, R. D., "Multi-Objective Hypersonic Entry Aeroshell Shape Optimization," *Journal of Spacecraft and Rockets*, Vol. 46, No. 5, 2009.

[11]Kinney, D. J., "Aerodynamic Shape Optimization of Hypersonic Vehicles," AIAA 2006-239, *44th AIAA Aerospace Sciences Meeting and Exhibit*, Reno, NV, 9-12 Jan. 2006.

[12]Mathematica, Ver. 7, Wolfram Research, Champaign, IL.

[13]Grant, M. J. and Braun, R. D., "Analytic Hypersonic Aerodynamics for Conceptual Design of Entry Vehicles," AIAA 2010-1212, *48th AIAA Aerospace Sciences Meeting Including the New Horizons Forum and Aerospace Exposition*, Orlando, FL, 4-7 Jan. 2010.

[14]Grant, M. J., *Rapid Simultaneous Hypersonic Aerodynamic and Trajectory Optimization for Conceptual Design*, PhD Thesis, Georgia Institute of Technology, School of Aerospace Engineering, May 2012.

[15]Grant, M. J. and Braun, R. D., "The Extension of Analytic Hypersonic Force Coefficients for Conceptual Design Using the Divergence Theorem," AIAA 2012-4580, *AIAA Atmospheric Flight Mechanics Conference and Exhibit*, Minneapolis, MN, 13-16 Aug. 2012.

[16]Grant, M. J., "The Construction of Analytic Hypersonic Pitch Moment Coefficients Using a Curl Transformation," AIAA 2013-0225, *51st AIAA Aerospace Sciences Meeting including the New Horizons Forum and Aerospace Exposition*, Grapevine, TX, 7-10 Jan. 2013.

[17]Hoffman, S. J. and Kaplan, D. I., "Human Exploration of Mars: The Reference Mission of the NASA Mars Exploration Study Team," *NASA Special Publication 6107*, July 1997.

[18]Drake, B. G., "Reference Mission Version 3.0 Addendum to the Human Exploration of Mars: The Reference Mission of the NASA Mars Exploration Study Team," *NASA Special Publication 6107-ADD*, June 1998.

[19]Steinfeldt, B., Theisinger, J., Korzun, A., Clark, I., Grant, M., and Braun, R., "High Mass Mars Entry Descent and Landing Architecture Assessment," AIAA 2009-6684, *AIAA Space 2009*, Pasadena, CA, 14 - 17 Sept. 2009.

[20]Desai, P., Lyons, D., Tooley, J., and Kangas, J., "Entry, Descent, and Landing Operations Analysis for the Stardust Entry Capsule," *Journal of Spacecraft and Rockets*, Vol. 45, No. 6, 2008.

[21]Desai, P. and Lyons, D., "Entry, Descent, and Landing Operations Analysis for the Genesis Entry Capsule," *Journal of Spacecraft and Rockets*, Vol. 45, No. 1, 2008.

[22]Kinney, D. J. and Bowles, J. V., "Conceptual Design of a 'SHARP'-CTV," AIAA 2001-2887, *35th AIAA Thermophysics Conference*, Anaheim, CA, 11-14 Jun. 2001.

[23]Grant, M. J., Clark, I. G., and Braun, R. D., "Rapid Design Space Exploration for Conceptual Design of Hypersonic Missions," *AIAA Atmospheric Flight Mechanics Conference and Exhibit*, Portland, OR, 8-11 Aug. 2011.

[24]Grant, M. J., Clark, I. G., and Braun, R. D., "Rapid Simultaneous Hypersonic Aerodynamic and Trajectory Optimization Using Variational Methods," AIAA 2011-6640, *AIAA Atmospheric Flight Mechanics Conference and Exhibit*, Portland, OR, 8-11 Aug. 2011.

[25]Rogers, D. F., *An Introduction to NURBS: With Historical Perspective*, Academic Press, London, 2001.